IEEE Access
Multidisciplinary | Rapid Review | Open Access Journal

Received January 21, 2022, accepted February 24, 2022, date of publication March 4, 2022, date of current version March 11, 2022.

*Digital Object Identifier 10.1109/ACCESS.2022.3157063*

# Measurement and Evaluation of 28 GHz Propagation Characteristics in Specific Environments

**SATOSHI ITO AND TAKAHIRO HAYASHI**
Radio and Spectrum Laboratory, KDDI Research, Inc., Saitama 356-8502, Japan

Corresponding author: Satoshi Ito (si-itou@kddi.com)

This work was supported by the Ministry of Internal Affairs and Communications in Japan.

**ABSTRACT** New specific scenarios are expected for 5G systems in various environments, such as stadiums, subway platforms, factories, livestock barns. On the other hand, the applicability of conventional propagation models to new specific environments has not been clarified. In this paper, we report path loss and spatiotemporal characteristics such as delay spread (DS) and azimuth and zenith angular spread of arrival (ASA and ZSA) in the 28 GHz-band in various environments. By comparing the degree of fit to the conventional models, we considered whether the models for conventional scenarios assumed by previous mobile systems can be applied to the propagation characteristics in each specific environment. As a result, we clarify that the following points should be considered when applying the conventional model. The measured path loss characteristics were mostly close to those of the conventional models. However, the path loss in the non-line-of-sight with propagation to another room was larger than the conventional model, assuming there was a hall space environment with some blockers. Regarding the DS, we obtained the results that the characteristics were mainly affected by existence of long-distance delayed wave caused by a long narrow space and materials of the internal walls and ceiling. Larger ASA characteristics were obtained in the subway platform environment and the factory environment because of metallic obstacles and walls. Regarding the ZSA, a larger ZSA was obtained in the stadium due to scattering from spectator seats, and a smaller ZSA was obtained in the subway platform due to the low ceiling height and long propagation distance.

**INDEX TERMS** 5G mobile communication system, millimeter-wave band, radio wave propagation, path loss, delay spread, angular spread.

## I. INTRODUCTION

The traffic load and the number of devices connected to mobile networks have increased rapidly because of the spread of smartphones [1]. To process the increased traffic and adapt new additional demands, a commercial service of the fifth-generation mobile communication system (5G system) was started in 2020 in Japan. Enhanced Mobile Broadband (eMBB), massive Machine Type Communication (mMTC) and Ultra-Reliable and Low Latency Communications (URLLC) were standardized as IMT-2020 by the International Telecommunication Union Radiocommunication (ITU-R) Sector [2]. Due to features other than the conventional high data rate and high capacity, such as ultra-multiple connections, ultra-reliability, and ultra-low latency by mMTC or URLLC, the 5G system is expected to be used for new specific scenarios in new specific environments such as stadiums, subway platforms, factories, and livestock barns [3]–[10]. We show concrete scenarios other than those of conventional use by the 5G system.

In stadiums, improving the experience value by broadcasting rich video content via the 5G system is considered [3]–[5]. A demonstration experiment was conducted to distribute a free viewpoint video, which was created by combining images shot by multiple cameras, to a large number of tablet devices.

In subway platforms, enhancement of the security system with a high-resolution video via the 5G system is considered [6]. This system transmits images from fixed cameras installed on subway platforms and 4K cameras mounted on

The associate editor coordinating the review of this manuscript and approving it for publication was Vittorio Degli-Esposti.

robot patrolling platforms to monitors or VR (Virtual Reality) goggles. 4K images are collected and analyzed by a server, which is expected to improve security by detecting knives that could not be detected with conventional image quality.

In factories, real-time remote control of factory machinery is being considered in order to improve productivity and safety [7]–[9]. In addition, for the quality control of products being manufactured, a scenario of remote control by transmitting images and videos captured by high-resolution cameras via the 5G system is also being considered.

In livestock barns, 4K images of dairy cows being fed were transmitted in real time via 5G, and from the images, the location of the dairy cows was identified by reading the ear mark with the individual identification number printed on it [10]. This is expected to efficiently identify the whereabouts of dairy cows in poor health.

On the other hand, the 5G systems also use millimeter-wave bands in addition to conventional frequency bands below 6 GHz. Since the millimeter-wave bands have a wider bandwidth than lower frequency bands allocated to conventional cellular systems, it is possible to achieve the high capacity communications required for the 5G system [11], [12]. In Japan, 5G commercial services have been launched using the 3.7 GHz band and the 28 GHz band [13]. The millimeter-wave band has a short propagation range due to larger propagation loss. Furthermore, it is easily affected by building structures and blocking objects due to its higher reflection and diffraction losses [14], [15]. Because of this, the propagation characteristics in the millimeter-wave band more significantly depend on the surrounding environment than in the lower frequency bands. Therefore, it is necessary to identify a propagation model that is more suitable for each specific environment.

Propagation characteristics in the millimeter-wave band have been reported and specified in [16]–[21]. Reference [16] reported the path loss characteristics of 26-, 32- and 39-GHz bands in an outdoor small-cell environment. [17] reported path loss characteristic of 28 and 39 GHz band in suburban environments. Reference [18] reported on the spatiotemporal characteristics of the 28 GHz band in classroom, office and hall environments. Reference [19] reported the path loss characteristics of a 60 GHz band in office environment. The Urban Micro (UMi) model, Urban Macro (UMa) model, and Indoor Hotspot (InH) model are specified in ITU-R M.2412 as propagation models for conventional cellular systems [20]. The UMi model and UMa model are for urban microcell and macrocell environments, and the InH model is for an indoor office environment. The Indoor Factory (InF) model, specified in 3rd Generation Partnership Project (3GPP) TR38.901 [21], is a model that assumes an indoor factory environment. These reports and models can provide a path loss and spatiotemporal characteristics in the millimeter-wave band, while the new usage scenarios envisioned in the 5G system are different from those envisioned in these previous reports and models.

In addition to the above propagation models for offices, classrooms and outdoor environments where wireless communication systems have been mainly used, propagation characteristics in new environments where millimeter waves are expected to be used have been reported [22]–[27]. In [22]–[24], channel characteristics were investigated at high-speed railway stations in the 28 GHz or 39 GHz band based on ray tracing simulations. On the other hand, further verification is needed to clarify the applicability in real environments, because these reports were based on simulation results by ray tracing. In [25] and [26], propagation characteristics, including spatiotemporal characteristics in real environments, were reported. [25] reported a delay profile and angular profile in the 1.4 GHz band in a stadium environment. Reference [26] reported the blockage loss characteristics of the human body in a 28 GHz band by reproducing a part of an indoor stadium environment. These reports indicated the propagation characteristics in environments where new applications are expected. However, since the frequency bands were different or the focus was on human blockage and not on statistical characteristics within a site, further verification is required for application in new usage scenarios. In [27] and [28], the results of wideband measurements in the 28 GHz band and 30GHz band in an indoor industrial environment were reported, and the propagation loss, DS and AS were reported. In [27] and [28], statistical propagation characteristics were reported, but indoor propagation characteristics vary specifically depending on object placement, indoor structure, etc. Therefore, more measurement results at more sites are needed to clarify the applicability. In addition, although the factory environment is similar to the indoor laboratory environment in terms of object type and size, the propagation characteristics are expected to be different in environments, such as stations or livestock barns due to the different object types. Therefore, it is necessary to clarify the applicability of conventional models to new specific scenarios in each environment.

In this paper, we report the statistical analysis results of the path loss and spatiotemporal characteristics, such as delay spread and angular spread, in the 28 GHz band in stadium, subway platform, factory, and livestock barn environments where use of the 5G system is expected.

The stadium environment differs from the conventional outdoor environment in terms of being surrounded by mortar-shaped spectator seats. In addition, the subway platform and livestock barn environment differ from conventional indoor environments, such as offices and factories, in terms of the density or type of obstacles. Moreover, various factories actually exist in terms of size, height, and clutter density, although the InF model was defined to provide propagation characteristics in the factory environment. Thus, it is necessary for us to clarify whether the InF model can also apply to each specific factory. The propagation characteristics of each environment are compared with the free space path loss (FSPL) and the UMi model, UMa model, InH model and InF model, and the suitability of the models is discussed.

This paper is organized as follows. Section II explains the measurement specifications and the processing of the measured data. Section III explains each measurement environment. Section IV describes the measured results of the path loss and the spatiotemporal characteristics for each environment. In Section IV, A, B, C and D describe the stadium environment, the subway platform environment, the factory environment, and the livestock barn environment, respectively. In addition, Section IV-E shows the summary of the results obtained at the four environments. Finally, we present our conclusions in Section V.

## II. MEASUREMENT METHOD

### A. MEASUREMENT PARAMETERS

Figure 1 shows a photograph of the measurement setup, and Table 1 shows the configurations of the measurement. The transmitter shown in Fig. 1(a) consists of a signal generator (SG), a low pass filter (LPF), an up-converter, a high power amplifier (HPA), a transmission antenna and coaxial cables connecting each device. IF signal of 1.45 GHz generated at the SG is input to LPF. After harmonic waves was removed by LPF, IF signal is up-converted to 28 GHz-band by the up-converter. The up-converted 28 GHz-band signal is amplified by the HPA and is input to the transmission antenna. The transmission antenna was a sleeve antenna with a 0.0 dBi gain including transmission loss by integrated input cable, and the transmission power was 35 dBm. The transmission antenna was mounted at heights of 16 m and 20 m in the stadium, 2.8 m in the subway platform, 2.5 m in the factory and 3.0 m, 6.0 m and 10.0 m in the livestock barn. The measurement frequency band was the 28 GHz band, and its center frequency was 27.925 GHz.

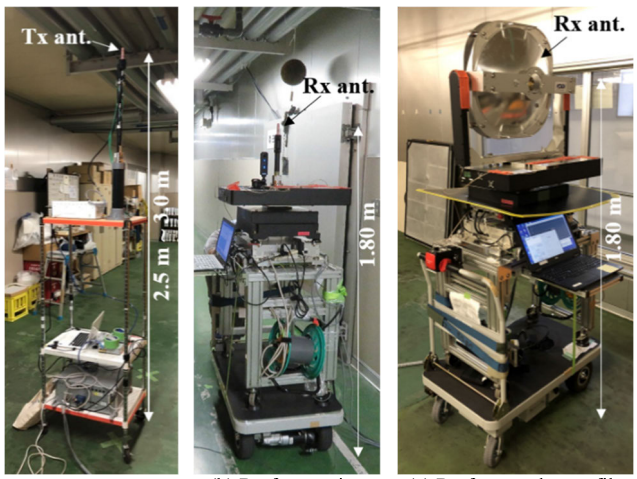


(a) Tx (b) Rx for moving measurement (c) Rx for angular profile measurement

**FIGURE 1.** Tx and Rx equipment photographs. The left side (a) shows transmission equipment setup. The center (b) shows the receiver equipment setup for the measurement of path loss and power delay profiles. The right side (c) shows the receiver equipment setup for the measurement of angular profiles.

**TABLE 1.** Measurement configurations.

| | Path loss | Delay Profile | Angular Profile |
|---|---|---|---|
| Center Freq. | 27.925 GHz | | |
| Emitting power | 35 dBm | | |
| CW/Modulated wave | CW | Modulated wave | CW |
| Bandwidth | - | 100 MHz | - |
| Tx antenna type (including input cable loss) | Sleeve Antenna (0.0 dBi) | | |
| Tx antenna polarization | Vertical pol. | | |
| Rx antenna type (including input cable loss) | Sleeve Antenna (0.0 dBi) | | Cassegrain Antenna (36.3 dBi) |
| Rx antenna polarization | Vertical pol. | | |
| Meas. Method | Moving measurement of 1.23 m/s | | Fixed point measurement |
| Meas. interval | Measured per 10 ms | | Measured per 2 degrees |

### B. PATH LOSS MEASUREMENT AND PROCESSING

The path loss characteristic was measured by walking the measurement route determined for each measured environment. Continuous waves were transmitted from each Tx point. While the receiving antenna was moved at a constant speed of 1.23 m/s by an electric hand truck, the received power was measured every 10 ms. The receiving antenna was a sleeve antenna with a 0.0 dBi gain including transmission loss by integrated input cable as shown in Fig. 1 (b). The moving median method was applied with a 1-m short window to remove the effect caused by fast fading. The path loss is given by equation (1):

$$PL_{meas} = P_{tx} + G_{tx} - P_{rx} + G_{rx} \tag{1}$$

$P_{tx}$, $G_{tx}$, $P_{rx}$, and $G_{rx}$ are the transmission power in dBm, Tx antenna gain in dBi, received power in dBm and Rx antenna gain in dBi, respectively. The path loss characteristics measured in each environment were regressed by the least squares methods for the single-frequency close-in (CI) free space reference distance model [29] given by equation (2).

$$PL_{fitting} = 61.37 + \alpha \log_{10} d \tag{2}$$

The slope $\alpha$ (based on regression) describes the distance $d$ between a transmitter and a receiver in each environment. Note that 61.37 is FSPL in dB at the 1 m point from a transmission point at 27.925 GHz. In this paper, the RMSE is used as a parameter in order to evaluate applicability of each model.

### C. MEASUREMENT AND PROCESSING OF SPATIOTEMPORAL CHARACTERISTICS

In the measurement campaigns in each environment, the delay spread (DS), azimuth angular spread of arrival (ASA), and zenith angular spread of arrival (ZSA) were measured.

This section describes the measurement and processing methods. We derived them based on the widely accepted WINNER II/3GPP channel model [30], [31].

#### 1) DELAY SPREAD

The delay profile was measured by walking the measurement route determined for each measured environment. Waves modulated by OFDM were transmitted from each Tx point. While the receiving antenna was moved at a constant speed of 1.23 m/s by an electric hand truck, the delay profile was measured every 10 ms. The receiving antenna was a sleeve antenna with a 0.0 dBi gain, as shown in Fig. 1 (b).

The DS $\sigma_\tau$ was derived from the measured delay profiles by equation (3):

$$\sigma_\tau = \sqrt{\frac{\int_0^\infty (\tau - \tau_m)^2 P_{delay}(\tau)\, d\tau}{\int_0^\infty P_{delay}(\tau)\, d\tau}} \tag{3}$$

$p(\tau)$ indicates the measured delay profile and $\tau$ indicates the delay time in seconds. After applying the moving-average method with a 1-m short window to remove the effect caused by fast fading for the measured delay profile, the values that were 5 dB higher than the average noise floor and within 20 dB of the maximum peak were extracted and used for the evaluation. The mean delay time $\tau_{\mathrm{m}}$ in seconds is given by equation (2):

$$\tau_m = \frac{\int_0^\infty \tau P_{delay}(\tau)\, d\tau}{\int_0^\infty P_{delay}(\tau)\, d\tau} \tag{4}$$

#### 2) ANGULAR SPREAD

The angular profiles were measured at fixed Rx points in each environment. Continuous waves were then transmitted from each Tx point, and they were measured at each Rx point by swinging a directional antenna. Fig. 1 (c) shows the receiver equipment setup for the measurement of the angular profiles. The receiving antenna was a Cassegrain antenna of a 36.3 dBi gain including transmission loss by integrated input cable, and the height of the receiving antenna was 1.8 m. The half power beamwidths in the horizontal and vertical planes were 1.5 degrees and 1.4 degrees, respectively. The rotation step was 2 degrees in the horizontal and vertical planes.

The angular spread $\sigma_{as}$ was derived from the measured angular profile $P_{ang}(\phi)$ by equation (5):

$$\sigma_{as} = \sqrt{\frac{\int_{\phi_1}^{\phi_2} (\phi - \phi_m)^2 P_{ang}(\phi)\, d\phi}{\int_{\phi_1}^{\phi_2} P_{ang}(\phi)\, d\phi}} \tag{5}$$

where $\phi$ indicates the azimuth and zenith angle of arrival. After adding the power in the horizontal or vertical direction for the measured angular profile, the values that were 5 dB higher than the average noise floor and within 20 dB of the maximum peak were extracted and used for the evaluation. The mean angle $\phi_m$ in the radian is given by (6):

$$\phi_m = \frac{\int_{\phi_1}^{\phi_2} \phi P_{ang}(\phi)\, d\phi}{\int_{\phi_1}^{\phi_2} P_{ang}(\phi)\, d\phi} \tag{6}$$

Note that $(\phi_1, \phi_2)$ in (5) and (6) are $(-\pi, \pi)$ in ASA and $(0, \pi)$ in ZSA. In addition, the smallest value of those calculated with the reference angle changed was used as ASA because of the periodicity of the azimuth angle.

## III. MEASUREMENT ENVIRONMENTS

### A. STADIUM ENVIRONMENT

Figure 2 and Figure 3 show the measurement map and a photograph of the stadium, respectively. Table 2 shows the measured positions of the fixed-point measurement for the angular spread. The measurement campaign was conducted in the stadium used for baseball. The transmitter was placed in the spectator seat area and in a lighting tower where the actual base station installation was assumed to be. The receiver was moved in the spectator seat area along the measurement routes. Tx1 in the spectator seat area and Tx2 by the lighting

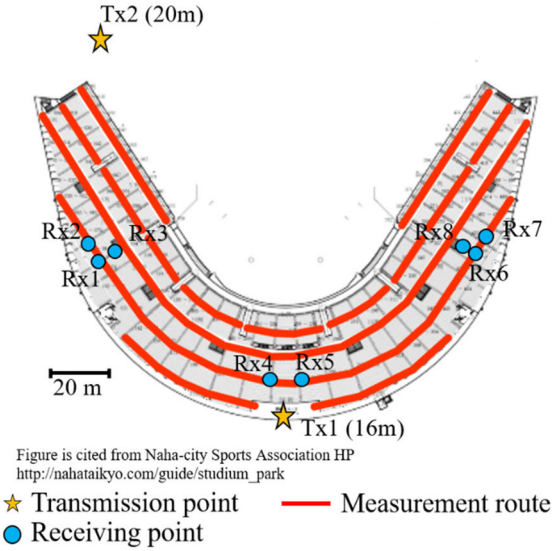


**FIGURE 2.** A map of the measured stadium environment.


**FIGURE 3.** A photograph of the measured stadium environment. Tx2 shown in the photograph was placed at a height of 20 m by a bucket vehicle.

**TABLE 2.** Tx-Rx positions for angular spread in the stadium.

| | Tx1 | Tx2 |
|---|---|---|
| Rx1 | ✓ | ✓ |
| Rx2 | | ✓ |
| Rx3 | | ✓ |
| Rx4 | | ✓ |
| Rx5 | | ✓ |
| Rx6 | ✓ | ✓ |
| Rx7 | ✓ | ✓ |
| Rx8 | ✓ | ✓ |

tower were installed at heights of 16 m and 20 m above the ground, respectively. The stadium environment was free of obstacles, as shown in Fig. 3, and all of this measurement environment was in a line-of-sight (LOS) environment. The InH and InF models are applied for indoor scenarios, and the UMi and UMa and RMa are applied for outdoor scenarios. This stadium environment is an open outdoor environment and is not an indoor environment. In addition, the UMi and UMa models assume that the urban environment is affected by buildings, while the RMa model assumes that the rural environment is affected by terrain, such as mountains. The stadium environment is surrounded by artificial materials, such as spectator seats, not terrain. Therefore, we compared it with the UMi and UMa models, which are considered to be more similar environments than the other models in TR38.901.

### B. SUBWAY PLATFORM ENVIRONMENT

Figure 4 shows the measurement environment of the subway platform, Figure 5 shows a photograph of the subway platform, and Table 3 shows the measured positions of the fixed-point measurement for angular spread. The measurement campaign was conducted in the subway platform shown in Fig. 4 and Fig. 5. Since the ceiling height of the platform is approximately 3.0 m and the access point is expected to be installed on the ceiling, the transmission antenna for the measurement campaign was mounted at a height of 2.8 m. In this environment, there are some metallic scatterers, such as platform doors and electric boards. In addition, this measurement campaign was conducted in an environment where

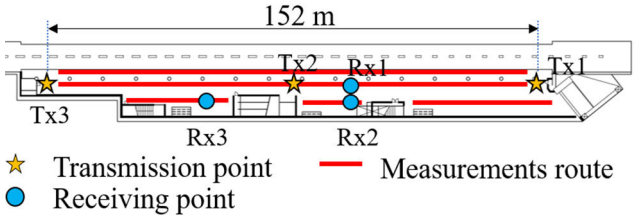


**FIGURE 4.** A map of the measured subway platform environment.


**FIGURE 5.** A photograph of the measured subway platform environment, which was taken from point Tx1.

**TABLE 3.** Tx-Rx positions for angular spread in the subway platform.

| | Tx1 | Tx2 | Tx3 |
|---|---|---|---|
| Rx1 | ✓ | | |
| Rx2 | ✓ | | |
| Rx3 | ✓ | ✓ | |

there were no train cars or passengers, using the period from the last train to the first train. As shown in Fig. 5, there are few obstacles in the environment. However, there are many areas that are blocked by pillars and electric boards. Due to a low blocking ratio and similar characteristics to the surrounding LOS areas in the blocked areas, the subway platform was classified as a LOS environment for all areas. Since this measurement environment is an indoor environment, it was compared with the InH and InF models, which are considered to be close to the environment.

### C. FACTORY ENVIRONMENT

Figure 6 shows the measurement environment of the factory. Figure 7 is a photograph of the inside of the factory taken from Rx5 in Fig. 6. Table 4 shows the measured positions of the fixed-point measurement for angular spread. The measurement campaign was conducted in a factory where sake (Japanese liquor) is produced. The factory is a closed indoor space with a metallic ceiling and walls. Room 1 shown in Fig. 6 is connected to the other room (Room 2) by a door. In this measurement campaign, the door connecting Room 1 and Room 2 was always open because the internal walls of this factory consisted of metallic material and little penetration through the metallic wall can exist. Actually, the propagation loss from Room 2 to Room 1 increased substantially when the door was closed. The ceiling height of this environment is approximately 3.0 m. The transmitting antenna was placed at a height of 2.5 m to avoid piping, with

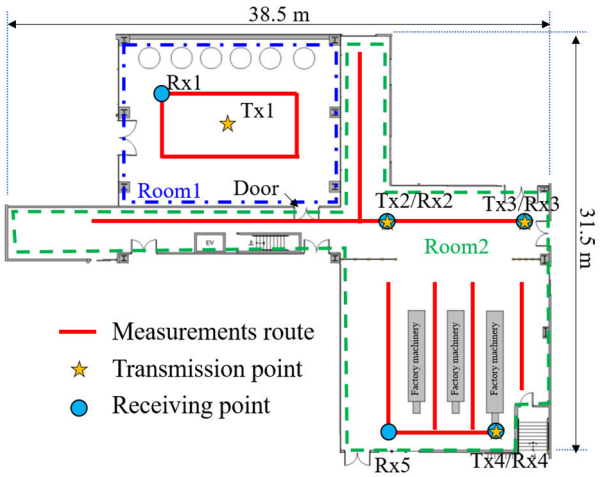


**FIGURE 6.** A map of the measured factory environment.

**FIGURE 7.** A photograph of the measured factory environment, which was taken from point Rx5.

**TABLE 4.** Tx-Rx positions for angular spread in the factory.

| | Tx1 | Tx2 | Tx3 | Tx4 |
|---|---|---|---|---|
| Rx1 | ✓ | ✓ | | |
| Rx2 | ✓ | | ✓ | ✓ |
| Rx3 | | ✓ | | ✓ |
| Rx4 | | ✓ | ✓ | |
| Rx5 | | | ✓ | ✓ |

the expectation that the access point would be installed on the ceiling.

As shown in Fig. 7, the measurement environment has many metallic obstacles and pipes. In this environment, we classified the non-line-of-sight (NLOS) area into two types. The first type of area is the NLOS, where the propagation was blocked by building structures, such as walls, and the second type of area is the NLOS, where the propagation was not blocked by walls but by some obstacles, such as factory machinery. In this paper, the first type of NLOS is described as NLOS-W. Since this measurement campaign was conducted in the factory, the results were compared with the InF model defined in the factory environment. The path loss of the InF model in NLOS depends on the clutter density and the relative height of the BS to the clutter. Then it is classified into the SL (sparse clutter, low BS) model, DL (dense clutter, low BS) model, SH (sparse clutter, high BS) model, and DH (sparse clutter, high BS) model. In this measurement campaign, the SH and DH models were compared with the measured results because the transmitter was installed near the ceiling, which is higher than the clutter height.

### D. LIVESTOCK BARN ENVIRONMENT

Figure 8 shows the measurement environment in the livestock barn. A photograph of the inside of the livestock barn taken from Tx1 in Fig. 8 is shown in Figure 9. Table 5 shows the measured positions of the fixed-point measurement for the angular spread. This livestock barn environment has a triangular roof with a ceiling height of 13.6 m at the highest point and 7.2 m at the lowest point. The main clutter is

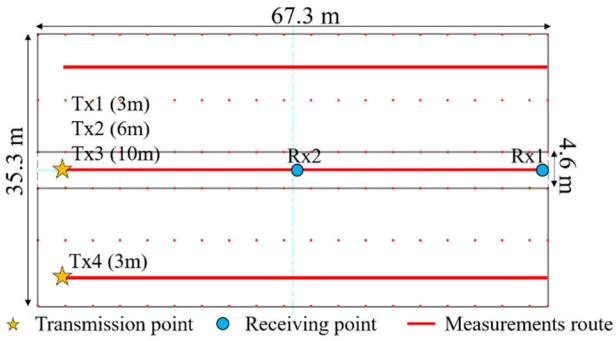


**FIGURE 8.** A map of the measured livestock barn environment.

**FIGURE 9.** A photograph of the measured livestock barn environment, which was taken from point Tx1.

**TABLE 5.** Tx-Rx positions for angular spread in the livestock barn.

| | Tx1 | Tx2 | Tx3 | Tx4 |
|---|---|---|---|---|
| Rx1 | ✓ | ✓ | ✓ | ✓ |
| Rx2 | ✓ | | | ✓ |

thin metallic objects, such as metallic pillars that stand at equal intervals of 3.5 m, and metallic fences on both sides of the center aisle. To obtain the characteristics of the actual livestock barn environment, this measurement campaign was conducted in a situation where there are some cows inside the livestock barn. Since this environment is an indoor environment, we compared it with the InH model and the InF model, which are considered to be similar environments.

## IV. MEASUREMENT RESULTS

### A. STADIUM ENVIRONMENT

#### 1) PATH LOSS CHARACTERISTICS

The distance characteristics of path loss in the stadium environment are shown in Figure 10. The values in the legend are the RMSE for each model.

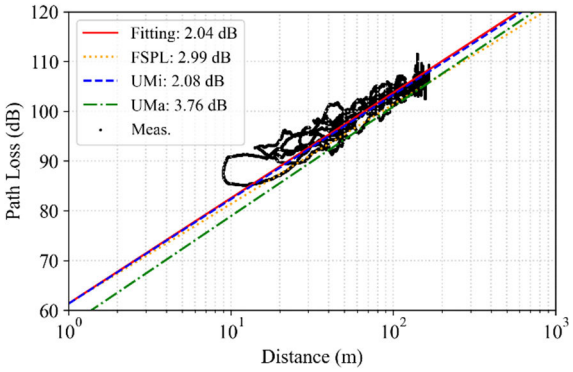


**FIGURE 10.** Distance characteristics of the path loss in the stadium environment.

The regressed slope $\alpha$ is 21.17, which is almost the same value as FSPL. The slope in the UMi model was 21, which gave almost the equivalent characteristics to the regressed model equation. The RMSE values for each model were 2.04 dB for the regression model, 2.99 dB for the FSPL, 2.08 dB for the UMi model, and 3.76 dB for the UMa model. Consequently, the UMi model was more suitable than the other conventional models. The RMSE value of 2.04 dB for fitting was smaller than the standard deviation of 4 dB for the shadow fading specified in the UMi model. This was considered to be caused by the stadium environment, which has no structures in the vicinity.

#### 2) SPATIOTEMPORAL CHARACTERISTICS

Figure 11 shows the cumulative probability distribution of the spatiotemporal characteristics in the stadium environment. Common logarithmic values log10 (DS/AS) are used as the x-axis. Fitting ($\mu/\sigma$), as shown by the red dotted line in the figures, describes the cumulative probability distribution of the normal distribution represented by the mean value $\mu$ and the standard deviation $\sigma$ of the measured values. Note that the number of measured AS samples is small for statistical values for angular spread. Figure 12 also shows an example of the angular profile of arrival in the stadium environment, where the transmitter is placed at Tx2 and the receiver is placed at Rx2.

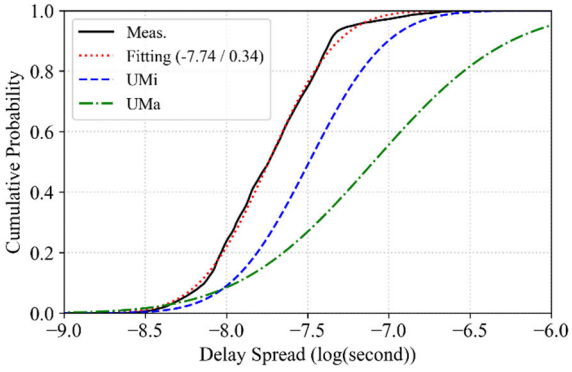


(a) DS

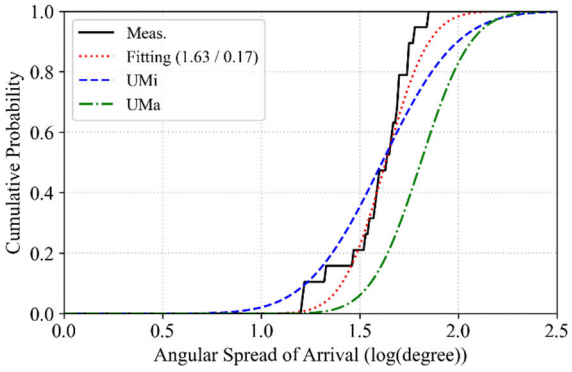


(b) ASA

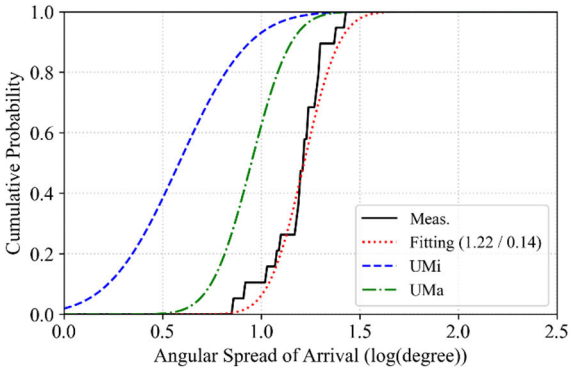


(c) ZSA

**FIGURE 11.** Cumulative probability distribution of spatiotemporal characteristics in the stadium environment.

The DS values shown in Fig. 11 (a) in the stadium environment are slightly smaller than those of the UMi model. The

UMi model assumes delayed waves due to structures, such as buildings. On the other hand, propagation in the stadium environment is mainly confined to the inside of the stadium. Therefore, the DS is considered to be small because there are few long-distance delayed waves.

The ASA values shown in Fig. 11 (b) in the stadium environment are equivalent to those of the UMi model, unlike the DS characteristics. In the stadium environment, the measurement campaign was conducted in the spectator seat area, and seats existed around the receiver. Therefore, scattered waves from the seats arrived strongly (other than the LOS wave), as shown in Figure 12. Hence, it is assumed that the measured ASA values became almost equal to those of the UMi model in the stadium environment due to the scattered waves from the seats.

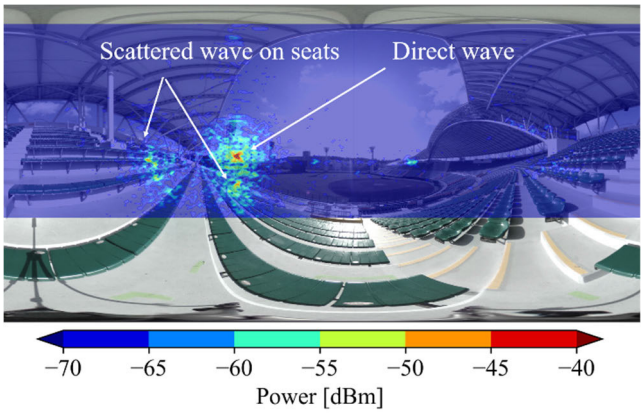


**FIGURE 12.** Arrival angular profile in the stadium environment where the transmitter was placed at Tx2 and the receiver was placed at Rx2.

The ZSA values shown in Fig. 11 (c) in the stadium environment are larger than those of the UMi and UMa models. This is considered to be the effect of scattered waves from the spectator seats as well as the ASA, as shown in Fig. 12. In addition, the propagation space in the stadium environment is smaller than the urban environment assumed in the UMi and UMa models, and the propagation distance is shorter than that in the urban environment. Therefore, the difference between the elevation angle of the sightlines and the elevation angle of the ground-reflected waves is larger than in urban areas, which is considered to statistically increase the ZSA values.

### *B. SUBWAY PLATFORM ENVIRONMENT*

#### 1) PATH LOSS CHARACTERISTICS

The distance characteristics of the path loss in the subway platform environment are shown in Figure 13. The values shown in the legend are the RMSE for each model. Fluctuations are caused by the shadow fading, not by the fast fading because the effect by fast fading was removed by the moving median process with 1-m short window.

The regressed slope $\alpha$ is 20.84, which is almost equivalent to FSPL. The slope in the InF model is 21.5, which gives

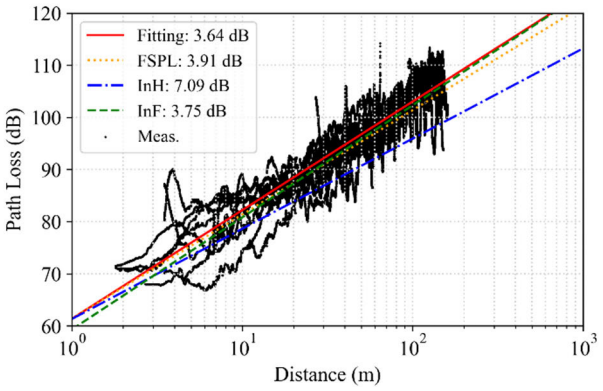


**FIGURE 13.** Distance characteristics of the path loss in the subway platform environment.

almost the equivalent characteristic to that of the regressed model equation. The RMSE values for each model are 3.64 dB for the regression model, 3.91 dB for the FSPL, 7.09 dB for the InH model, and 3.75 dB for the InF model. Consequently, the InF model was more suitable than other conventional models. The RMSE value of 3.64 dB for the fitting model was close to the standard deviation value of 3 dB and 4.3 dB for the shadow fading specified in the InH and InF models. This is because the main clutter in the subway platform environment is pillars and electric boards, which are comparable in size to factory machines assumed to be blocking objects in the InH and InF models. Furthermore, the InF model was more suitable than the InH model for the measured results. This is because the InH LOS model assumes an empty hall space without any obstacles, and blockage loss is considered by adapting the blockage model.

#### 2) SPATIOTEMPORAL CHARACTERISTICS

Figure 14 shows the cumulative probability distribution of the spatiotemporal characteristics in the subway platform environment. Common logarithmic values log10(DS/AS) are used as the x-axis. Fitting $(\mu/\sigma)$ in the figures is the cumulative probability distribution of the normal distribution represented by the mean value $\mu$ and the standard deviation $\sigma$ of the measured values. Note that the number of measured AS samples is small for statistical values for the angular spread. As an example of the angular profile of arrival in the subway platform environment, Figure 15 shows the angular profile when the transmitter is placed at Tx1, and the receiver is placed at Rx1.

The DS values and the ASA values shown in (a) and (b) of Fig. 14 in the subway platform environment were larger than those of the InH and InF models. This is because there are almost no obstacles to block the propagation, except for cylindrical pillars or electric boards, and long-distance delayed waves arrive from the far pillars and far walls without attenuation, as shown in Fig. 15. Therefore, wireless systems should be designed considering a large delay in a long-distance propagation environment with metallic obstacles.

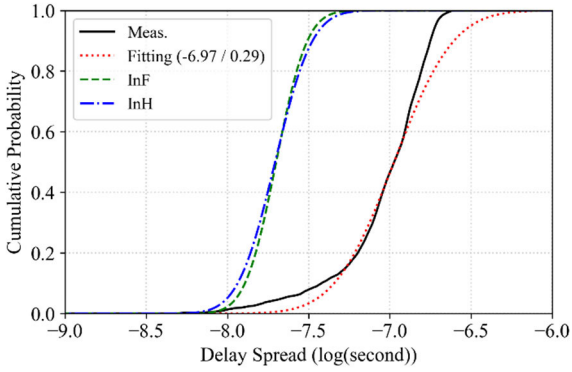


(a) DS

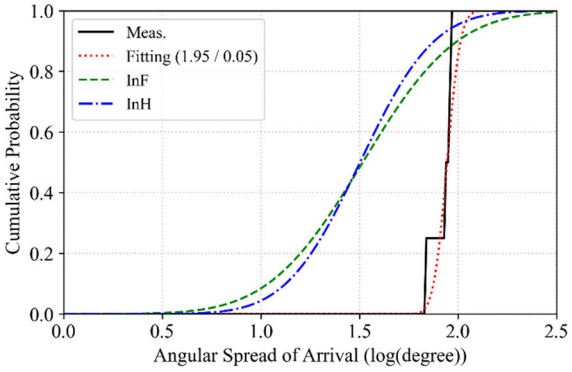


(b) ASA

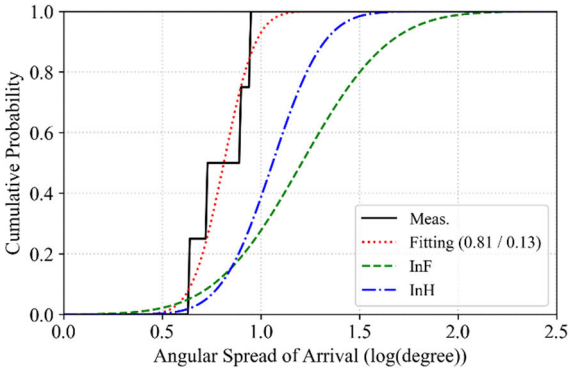


(c) ZSA

**FIGURE 14.** Cumulative probability distribution of spatiotemporal characteristics in the subway platform environment.

The ZSA values in the subway platform environment shown in Fig. 14 (c) are smaller than those of the InH and InF models. This is because the ceiling height of the subway platform environment was approximately 3.0 m, which is lower than the assumed ceiling height of 5 m to 25 m for the InF model. Therefore, the vertical multipath angle was limited by the ceiling and floor. Although the assumed ceiling height of the InH model is 3 m, this subway platform environment has many measurement points with a long propagation distance between the transmitter and receiver. The difference in the elevation angle between the direct wave and reflected waves

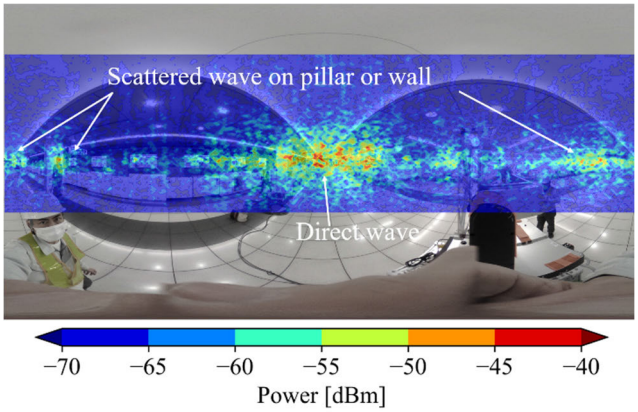


**FIGURE 15.** Arrival angular profile in the subway platform environment where the transmitter was placed at Tx1 and the receiver was placed at Rx1.

on the floor or the ceiling is smaller, which is thought to have resulted in a smaller ZSA.

### C. FACTORY ENVIRONMENT

#### 1) PATH LOSS CHARACTERISTICS

Figure 16 shows the distance characteristics of the path loss in a factory environment. The values in the legend are the RMSE for each model.

For the LOS shown in Fig. 16 (a), the regressed slope $\alpha$ is 20.36, which is almost equivalent to FSPL. In addition, the slope in the InF model was 21.5, giving almost the equivalent characteristics to those of the regressed model equation. The RMSE values for each model were 2.93 dB for the regression model, 2.95 dB for FSPL, and 3.30 dB for the InF model. The 2.93 dB RMSE value for fitting is smaller than the standard deviation of the 4.3 dB shadow fading specified in the InF model. Since the hall size assumed by the InF model is between 20 $m^2$ and 160,000 $m^2$, this factory environment is on the small side in the environment assumed by the InF model. As a result, the distance to the walls and clutter was short, and multipaths arrived without large attenuation in this environment. When a large number of multipaths arrive, the probability of large power degradation due to phase cancellation, as in the two-wave model, decreases, and the power distribution tends to be uniform in a hall. Therefore, the variation in the power is less than that of the InF model. The angular profile of arrival is described in detail in the spatiotemporal characteristics section.

For the NLOS shown in Fig. 16 (b), the regressed slope $\alpha$ was 23.4. The $\alpha$ slopes in the InF-SH and -DH models were 23.0 and 21.9, respectively, giving almost equivalent characteristics to those of the regressed model equation. The RMSE values for each model were 2.63 dB for the regressed model, 4.72 dB for the FSPL, 2.68 dB for the InF-SH model, and 2.75 dB for the InF-DH model. The RMSE value of 2.63 dB in the fitting was smaller than the standard deviation of shadow fading of 5.9 dB and 4.0 dB specified in the InF-SH and InF-DH models, respectively. This seems to be caused by

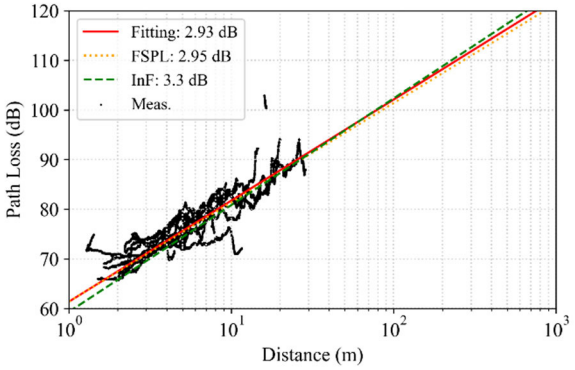


(a) LOS

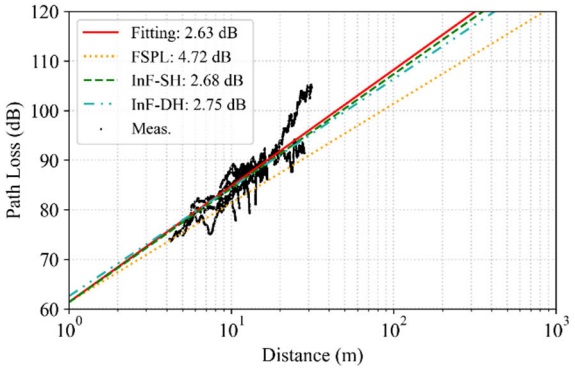


(b) NLOS, which was shadowed by some obstacles, such as factory machinery

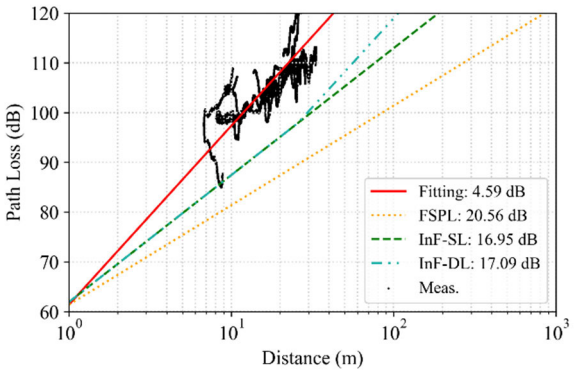


(c) NLOS-W, which was shadowed by building structures, such as a wall

**FIGURE 16. Distance characteristics of the path loss in the factory environment.**

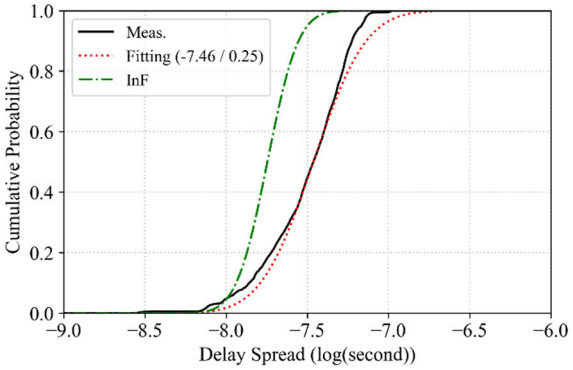


(a) DS

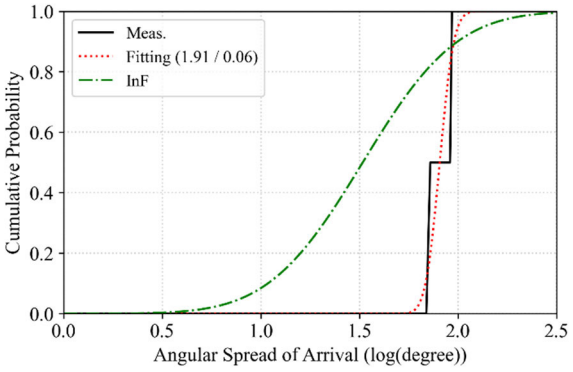


(b) ASA

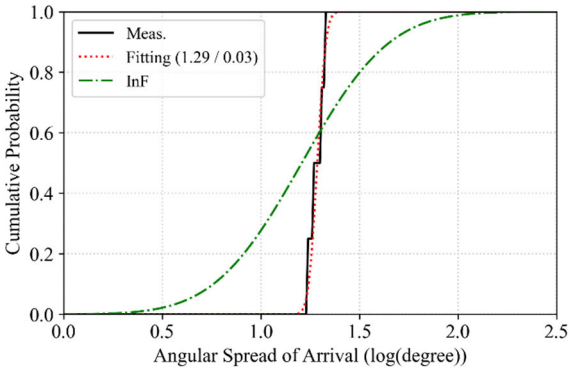


(c) ZSA

**FIGURE 17. Cumulative probability distribution of spatiotemporal characteristics in the factory LOS environment.**

the uniform power distribution in an environment with many multipaths, as with the LOS.

For NLOS-W shown in Fig. 16 (c), the regressed slope $\alpha$ was 35.96. The RMSE values for each model were 4.59 dB for the regression model, 20.56 dB for FSPL, 16.95 dB for the InF-SH model, and 17.09 dB for the InF-DH model. The $\alpha$ slope of 35.96 in fitting is larger than that of 23.0 and 21.9 in the InF-SH and InF-DH models. This is because the propagation in NLOS-W is different from that in the InF model, where the transmission wave propagates in a single hall space without walls. In addition, since there is no propagation path other than the path through a door in NLOS-W, it is not appropriate to apply the InF model, which uses the direct distance between the transmitter and receiver. In the case of propagation to another room, such as NLOS-W, it is important to apply a proper model that can represent the actual propagation mechanism, such as propagation via the door, penetration through the wall, etc.

### 2) SPATIOTEMPORAL CHARACTERISTICS

The spatiotemporal characteristics of the LOS and NLOS environments are shown in Figure 17 and Figure 18,

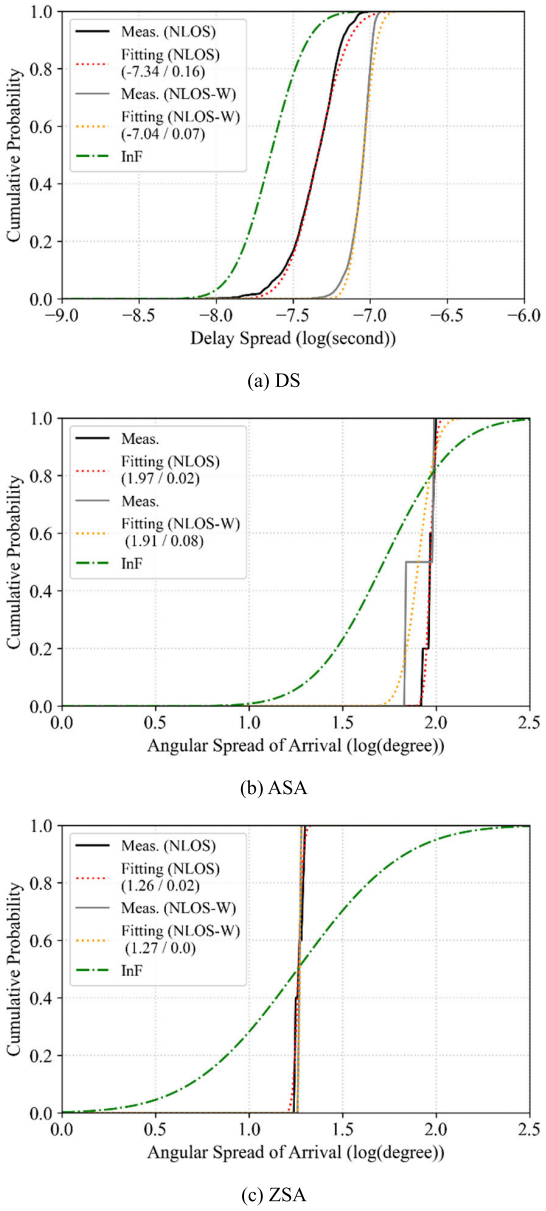


**FIGURE 18.** Cumulative probability distribution of spatiotemporal characteristics in the factory NLOS and NLOS-W environments.

respectively. Common logarithmic values log10(DS/AS) are used as the x-axis. Fitting $(\mu/\sigma)$ in the figures is the cumulative probability distribution of the normal distribution represented by the mean value $\mu$ and the standard deviation $\sigma$ of the measurements. Note that the number of measured AS samples is small for statistical values for angular spread. As an example of the angular profile of arrival in the factory environment, Figure 19 is the angular profile of arrival when the transmitter was placed at Tx2 and the receiver was placed at Rx4.

The ZSA values shown in Fig. 17 (c) and Fig. 18 (c) are close to the values of the InF model, while the DS values and the ASA values shown in (a) and (b) of Fig. 17 and Fig. 18 were larger than those of the InF models. The InF

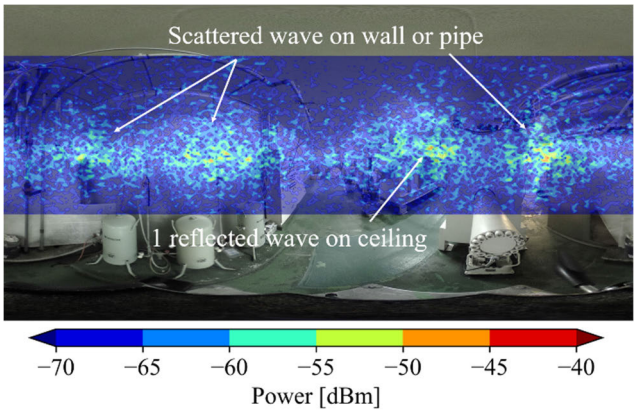


**FIGURE 19.** Arrival angular profile in the stadium environment where the transmitter was placed at Tx2 and the receiver was placed at Rx4.

model does not define a specific material of the internal wall and ceiling and assumes general material, such as concrete and metal, as the internal walls and ceiling. The internal wall and ceiling of this factory are metallic materials that provide the smallest reflection loss of all materials. Therefore, larger DS and ASA values were obtained by arriving at strong multipaths with a low additional loss. In addition, the mean values of the measured DS and ASA in the LOS and NLOS are larger than those reported in [27]. This is because there were many metallic objects with smallest reflection loss in this factory environment in comparison with the environment measured in [27].

For the DS in the NLOS shown in Fig. 18 (a), the value of DS in the NLOS-W was larger than that of the InF NLOS model. This is because the propagation in NLOS-W is limited to only the path via the door, and the radio waves are re-radiated at the point of the door with a width of 1 m. Since the InF model does not assume propagation to another room, it is considered difficult to apply the InF model in NLOS-W. Furthermore, a larger DS in NLOS-W was obtained compared with LOS and NLOS. In NLOS, blockage obstacles are mainly factory machinery and single reflected waves on the ceiling can arrive in NLOS. However, single reflected waves on the ceiling do not arrive in NLOS-W, because all paths propagate via the door, and even the path with the maximum received power arrives after multiple reflections. Therefore, the power difference between the maximum path and the other multipaths is smaller and the DS is larger in NLOS-W.

As shown in Fig. 19, many strong delayed waves arrived in the factory environment due to metallic clutter centrifugation. Because of the strong multipath environment, little variation in the received power was observed in this environment, as shown in Section IV-C-1.

### D. LIVESTOCK BARN ENVIRONMENT

#### 1) PATH LOSS CHARACTERISTICS

The distance characteristics of the path loss in the livestock barn environment are shown in Figure 20. The values in the legend are the RMSE for each model.

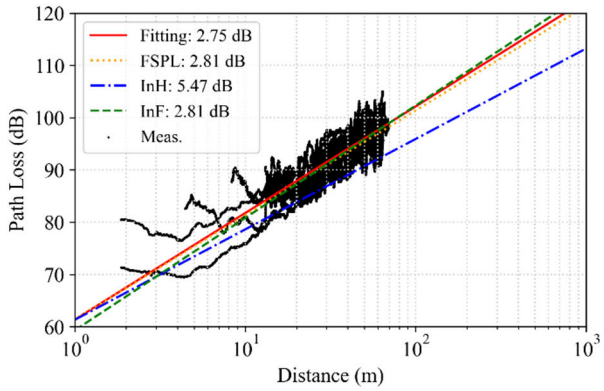


**FIGURE 20.** Distance characteristics of the path loss in the livestock barn environment.

The regressed slope $\alpha$ was 20.39, which is the equivalent value to the FSPL. The slope in the InF model was 21.5, which gave characteristics equivalent to those of the regressed model equation. The RMSE values for each model were 2.75 dB for the regression model, 2.81 dB for the FSPL, 5.47 dB for the InH model, and 2.81 dB for the InF model. Consequently, the InF model was more suitable than other conventional models. The RMSE value of 2.75 dB for the fitting was slightly smaller than the standard deviation of 3 dB and 4.3 dB for the shadow fading specified in the InH and InF models. The main clutter in the livestock barn environment is metallic pillars which are smaller than the clutter assumed by the InH and InF models, such as factory machinery. In addition, the metallic pillars were placed periodically throughout the livestock barn. Therefore, the livestock barn environment was more uniform than the environments of the InH and InF models because of the small deviation in the environment due to the large clutter. For these reasons, the variation in the path loss is considered to be smaller. Furthermore, the InF model was more suitable than the InH model for the measured results. This is because the InH model in the LOS does not assume any blocker, and the blockage loss is considered by additionally adapting the blockage model.

### 2) SPATIOTEMPORAL CHARACTERISTICS

Figure 21 shows the cumulative probability distribution of the spatiotemporal characteristics in the livestock barn environment. Common logarithmic values log10(DS/AS) are used as the x-axis. Fitting $(\mu/\sigma)$ in the figures is the cumulative probability distribution of the normal distribution represented by the mean value $\mu$ and the standard deviation $\sigma$ of the measured values. Note that the number of measured AS samples is small for statistical values for the angular spread. Figure 22 shows an example of the angular profile of arrival in the livestock barn environment, where the transmitter was placed at Tx4 and the receiver was placed at Rx1.

The characteristics of DS, ASA, and ZSA shown in Fig. 21 are all close to those of the InF model. This is because the environment assumed by the InF model is a hall

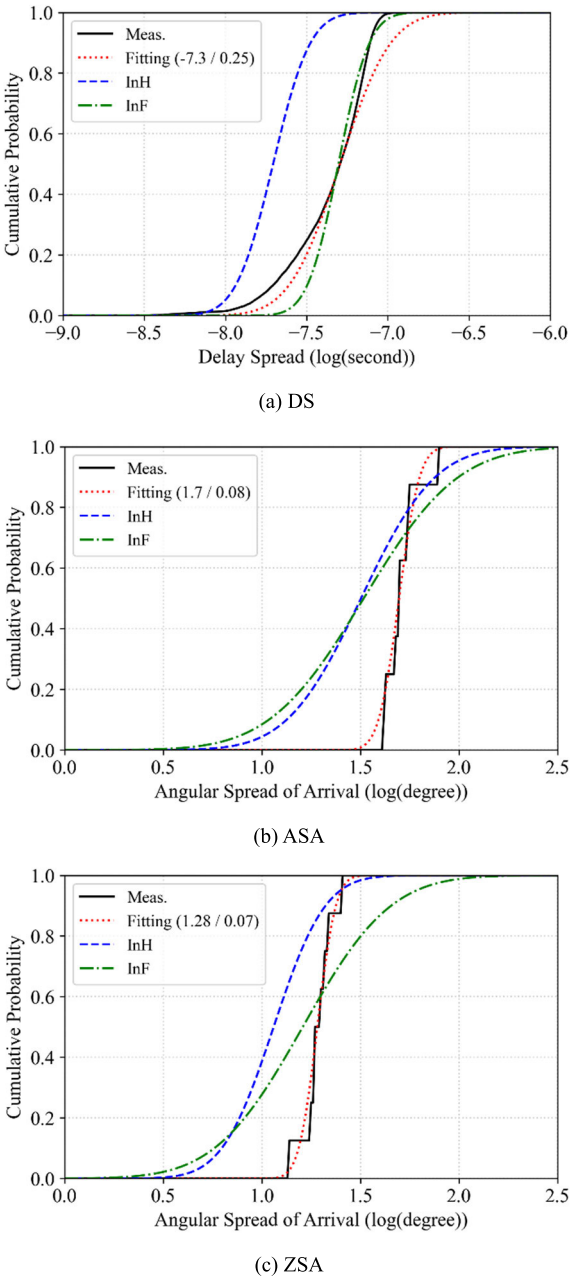


**FIGURE 21.** Cumulative probability distribution of spatiotemporal characteristics in the livestock barn environment.

room, which is similar to this measured environment. In addition to the direct wave, the angular profile in Fig. 22 indicates that reflections from the pillars and walls near the receiver arrived strongly, but there was little effect from the periodically-placed metallic pillars. In the case of the 75 m distance between the transmitter and receiver, the diameter of the first Fresnel zone at the center of the transmitter and receiver was approximately 82 cm. It is larger than the size of the metallic pillars. Therefore, no significant effect of periodically-placed pillars seems to be observed. In addition, little effect on the spatiotemporal characteristics caused by

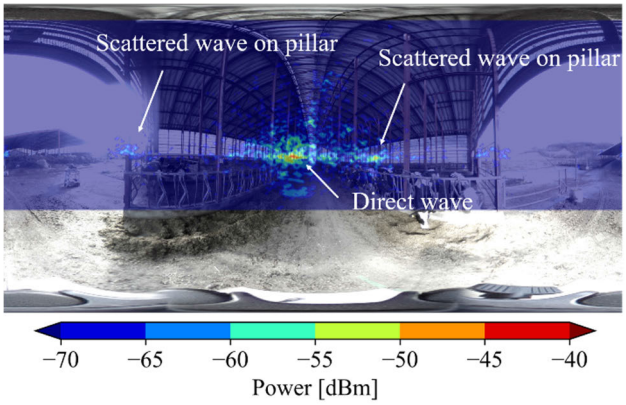


**FIGURE 22.** Arrival angular profile in the livestock barn environment where the transmitter was placed at Tx4 and the receiver was placed at Rx1.

cows was observed because the height of the cow was lower than the heights of Tx and Rx. Accordingly, small obstacles such as pillars or low obstacles such as cows have little effect.

### E. SUMMARY

Regarding the path loss, Table 6 shows the slope value $\alpha$ and the RMSE in each environment. In the LOS of the four environments we measured, the slope values ranged from 20.36 to 21.17, which is close to the free space path loss of 20. In the factory environment, the slope value was 23.40, which was close to the LOS value when Tx and Rx were placed in the same hall space and were not separated by a wall. However, when Tx and Rx were separated by a wall, the slope value was as large as 35.96 because the propagation path was longer without penetrating the metal wall.

**TABLE 6.** Path loss characteristics.

| | Visibility | Slope $\alpha$ | RMSE |
|---|---|---|---|
| Stadium | LOS | 21.17 | 2.04 dB |
| Subway Platform | LOS | 20.84 | 3.64 dB |
| Factory | LOS | 20.36 | 2.93 dB |
| | NLOS | 23.40 | 2.63 dB |
| | NLOS-W | 35.96 | 4.59 dB |
| Livestock Barn | LOS | 20.39 | 2.75 dB |

Regarding the DS, Table 7 shows the mean value and the standard deviation in each environment and model. As mentioned in Section IV-A to IV-D, we obtained the results that the characteristics were mainly determined by long-distance delayed waves. Regarding the stadium environment, the path of delayed waves is limited inside of a stadium. Therefore, a long-distance delayed wave scarcely arrives at a receiver, and DS tends to be small in a stadium environment. The subway platform environment is an indoor closed environment surrounded by walls, and there are few blockage obstacles.

**TABLE 7.** Delay spread characteristics.

| Environment | Visibility | Meas./Model | Mean | Standard dev. |
|---|---|---|---|---|
| Stadium | LOS | Meas. | -7.74 | 0.34 |
| | | UMi | -7.49 | 0.38 |
| | | UMa | -7.09 | 0.66 |
| Subway Platform | LOS | Meas. | -6.97 | 0.29 |
| | | InH | -7.71 | 0.18 |
| | | InF | -7.70 | 0.15 |
| Factory | LOS | Meas. | -7.46 | 0.25 |
| | | InF | -7.75 | 0.15 |
| | NLOS | Meas. | -7.34 | 0.16 |
| | | InF | -7.65 | 0.19 |
| | NLOS-W | Meas. | -7.04 | 0.07 |
| | | InF | -7.65 | 0.19 |
| Livestock Barn | LOS | Meas. | -7.30 | 0.25 |
| | | InH | -7.71 | 0.18 |
| | | InF | -7.30 | 0.15 |

**TABLE 8.** Angular spread characteristics.

| Environment | Visibility | Meas./Model | ASA (Mean/Std. dev.) | ZSA (Mean/Std. dev.) |
|---|---|---|---|---|
| Stadium | LOS | Meas. | 1.63/0.17 | 1.22/0.14 |
| | | UMi | 1.61/0.30 | 0.58/0.28 |
| | | UMa | 1.81/0.20 | 0.95/0.16 |
| Subway Platform | LOS | Meas. | 1. 95/0.05 | 0.81/0.13 |
| | | InH | 1.50/0.29 | 1.06/0.21 |
| | | InF | 1.52/0.38 | 1.21/0.35 |
| Factory | LOS | Meas. | 1.91/0.06 | 1.29/0.03 |
| | | InF | 1.52/0.38 | 1.21/0.35 |
| | NLOS | Meas. | 1.97/0.02 | 1.26/0.02 |
| | | InF | 1.72/0.30 | 1.26/0.45 |
| | NLOS-W | Meas. | 1.91/0.08 | 1.27/0.00 |
| | | InF | 1.72/0.30 | 1.26/0.45 |
| Livestock Barn | LOS | Meas. | 1.70/0.08 | 1.28/0.07 |
| | | InH | 1.50/0.29 | 1.06/0.21 |
| | | InF | 1.52/0.38 | 1.21/0.35 |

Hence, DS tends to be large in subway platform environment due to the low blockage loss.

In the factory environment, a larger DS in NLOS-W was obtained compared to LOS and NLOS. This is because the power difference between the maximum path and the other multipaths is smaller because single reflected waves on the ceiling do not arrive.

Regarding the AS, Table 8 shows the mean value and standard deviation in each environment and model. ASA is smaller in open environments, such as stadium environments, and ASA becomes larger in closed environments. On the other hand, the ZSA in a stadium environment is equivalent to that of a closed environment due to scattering from spectator seats behind a receiver. When compared with closed indoor environments, the ZSA is smaller in the subway platform. This is because the subway platform is an environment in which the distance between the transmitter and receiver is long, and the difference in the elevation angle between the direct wave and reflected waves on the floor or the ceiling is smaller. On the other hand, the number of samples is small due to the measurement time. Therefore, we think that additional verification is required to check the statistical validity and increase the effectiveness of the measured AS results.

## V. CONCLUSION

In this paper, we reported on the statistical propagation characteristics in the 28 GHz band in a stadium environment, a subway platform environment, a factory environment and a livestock barn environment expected to be used by the 5G system. In addition, the propagation characteristics in each environment were compared and evaluated with the conventional propagation model specified with 3GPP and ITU-R. Moreover, a discussion and analysis of the degree of fit between each environment and the conventional model were presented.

As a result, we clarified that the following points should be considered when applying the conventional model. For the path loss characteristics, the measured characteristics were mostly close to those of the conventional models. However, the measured path loss in NLOS-W in the factory environment was larger than that in the conventional model. This is because the propagation in NLOS-W is different from that in the InF model, where the radiated wave propagates in a single hall space without walls. In addition, since there is no propagation path other than the path through a door in NLOS-W, it is not appropriate to apply the InF model, which uses the direct distance between the transmitter and receiver. For the spatiotemporal characteristics, the measured characteristics have some differences from the conventional model due to the propagation environment. Regarding the DS, we obtained the results where the characteristics were mainly determined by long-distance delayed waves. For example, the DS in the stadium environment is smaller than that of the conventional model because the propagation path is mainly confined to the inside of the stadium. The DS in the subway platform environment is larger than that of the conventional model because there are almost no obstacles blocking propagation, except for the cylindrical pillars, and long-distance delayed waves arrive from the far pillars and far walls without attenuation. The measured ASA characteristics were mostly close to those of the conventional models, while the measured ZSA characteristic was larger than that of the conventional model in the stadium because of the scattered wave from spectator seats. In addition, the subway platform environment was smaller than that of the conventional model due to the low ceiling height and long propagation distance.

For future study, we plan to expand the number of measurement environments and try to consider a model in which the difference between each environment can be expressed as a function of some parameter.

## REFERENCES


[1] (Mar. 9, 2020). Cisco. *Cisco Annual Internet Report (2018–2023) White Paper*. [Online]. Available: https://www.cisco.com/c/en/us/solutions/collateral/executive-perspectives/annual-internet-report/white-paper-c11-741490.html

[2] *IMT Vision—Framework and Overall Objectives of the Future Development of IMT for 2020 and Beyond*, document ITU-R M.2083, ITU-R Recommendation, Sep. 2015.

[3] Huawei. (Oct. 2019). *Indoor 5G Scenario Oriented White Paper*. [Online]. Available: https://carrier.huawei.com/~/media/CNBGV2/download/products/servies/Indoor-5G-Scenario-Oriented-White-Paper-en.pdf

[4] M. Usami, "New world explored by 5G," in *Proc. IEEE Int. Conf. Consum. Electron. (ICCE)*, Las Vegas, NV, USA, Jan. 2020, p. 1, doi: 10.1109/ICCE46568.2020.9043147.

[5] K. Nonaka, R. Watanabe, J. Chen, H. Sabirin, and S. Naito, "Fast plane-based free-viewpoint synthesis for real-time live streaming," in *Proc. IEEE Vis. Commun. Image Process. (VCIP)*, Taichung, Taiwan, Dec. 2018, pp. 1–4, doi: 10.1109/VCIP.2018.8698648.

[6] (Oct. 2018). 5G Americas. *The Evolution of Security in 5G*. [Online]. Available: https://www.5gamericas.org/wp-content/uploads/2019/07/5G_Americas_5G_Security_White_Paper_Final.pdf

[7] *Study on Communication for Automation in Vertical Domains*, document TR 22.804, Jul. 2020.

[8] A. Yokota, S. Osada, S. Honda, K. Yamafuku, T. Nishida, T. Ikenaga, N. Mori, A. Matsunaga, K. Maruyama, and K. Yoshida, "Development of industrial robot system with 5th generation mobile communication system," in *Proc. 19th Int. Conf. Control, Autom. Syst. (ICCAS)*, Jeju, South Korea, Oct. 2019, pp. 851–855, doi: 10.23919/ICCAS47443.2019.8971662.

[9] B. Holfeld, D. Wieruch, T. Wirth, L. Thiele, S. A. Ashraf, J. Huschke, I. Aktas, and J. Ansari, "Wireless communication for factory automation: An opportunity for LTE and 5G systems," *IEEE Commun. Mag.*, vol. 54, no. 6, pp. 36–43, Jun. 2016.

[10] T. T. Zin, S. Misawa, M. Z. Pwint, S. Thant, P. T. Seint, K. Sumi, and K. Yoshida, "Cow identification system using ear tag recognition," in *Proc. IEEE 2nd Global Conf. Life Sci. Technol. (LifeTech)*, Kyoto, Japan, Mar. 2020, pp. 65–66, doi: 10.1109/LifeTech48969.2020.1570625232.

[11] (Mar. 2020). GSMA. *5G Spectrum Positions*. White Paper. [Online]. Available: https://www.gsma.com/spectrum/wp-content/uploads/2020/03/5G-Spectrum-Positions.pdf

[12] *New Frequency Range for NR (24.25-29.5 GHz)*, document TR 38.815, 3GPP TSG RAN, Jun. 2018.

[13] (Feb. 2021). *Ministry of Internal Affairs and Communications*. Current Situation of Spectrum Use in Japan. [Online]. Available: https://www.tele.soumu.go.jp/e/index.htm

[14] (Oct. 2016). Aalto University. AT&T, BUPT, CMCC, Ericsson, Huawei, Intel, KT Corporation, Nokia, NTT DOCOMO, New York University, Qualcomm, Samsung, University of Bristol, University of Southern California. *5G Channel Model for Bands up to 100 GHz (v2.3)*. [Online]. Available: http://www.5gworkshops.com/5GCM.html

[15] S. Sun T. S. Rappaport, T. A. Thomas, A. Ghosh, H. C. Nguyen, I. Z. Kovács, I. Rodriguez, O. Koymen, and A. Partyka, "Investigation of prediction accuracy, sensitivity, and parameter stability of large-scale propagation path loss models for 5G wireless communications," *IEEE Trans. Veh. Technol.*, vol. 65, no. 5, pp. 2843–2860, May 2016.

[16] M. Khalily, M. Ghoraishi, S. Taheri, S. Payami, and R. Tafazolli, "Millimeter-wave directional path loss models in the 26 GHz, 32 GHz, and 39 GHz bands for small cell 5G cellular system," in *Proc. 12th Eur. Conf. Antennas Propag. (EuCAP)*, 2018, pp. 1–5, doi: 10.1049/cp.2018.0376.

[17] P. Zhang, J. Li, H. Wang, and W. Hong, "Measurement-based propagation characteristics at 28 GHz and 39 GHz in suburban environment," in *Proc. IEEE Int. Symp. Antennas Propag. USNC-URSI Radio Sci. Meeting*, Atlanta, GA, USA, Jul. 2019, pp. 2121–2122, doi: 10.1109/APUSNCURSINRSM.2019.8889362.

[18] G. Zhang, k. Saito, W. Fan, X. Cai, P. Hanpinitsak, J.-I. Takada, and G. F. Pedersen, "Experimental characterization of millimeter-wave indoor propagation channels at 28 GHz," *IEEE Access*, vol. 6, pp. 76516–76526, 2018, doi: 10.1109/ACCESS.2018.2882644.

[19] M. Wang, Y. Liu, S. Li, and Z. Chen, "60 GHz millimeter-wave propagation characteristics in indoor environment," in *Proc. IEEE 9th Int. Conf. Commun. Softw. Netw. (ICCSN)*, Guangzhou, China, May 2017, pp. 749–752, doi: 10.1109/ICCSN.2017.8230211.

[20] *Guidelines for Evaluation of Radio Interface Technologies for IMT-2020*, document ITU-R M.2412-0, 2017.

[21] *Study on Channel Model for Frequencies from 0.5 to 100 GHz*, document TR 38.901 version 16.1.0 Release 16), 3GPP, [21] 3rd Generation Partnership Project, Jan. 2020. [Online]. Available: https://www.3gpp.org/ftp//Specs/archive/38_series/38.901/38901-g10.zip

[22] L. Xiong, H. Miao, B. Ai, T. Juhana, and A. Kurniawan, "Channel characteristics of high-speed railway station based on ray-tracing simulation at 5G mmWave band," *Int. J. Antennas Propag.*, vol. 2019, pp. 1–10, Sep. 2019, doi: 10.1155/2019/3137583.

[23] H. Miao and L. Xiong, "Channel characteristics of subway station based on ray-tracing at 5G mmWave band," in *Proc. IEEE/CIC Int. Conf. Commun. China (ICCC)*, Aug. 2020, pp. 687–692, doi: 10.1109/ICCC49849.2020.9238885.

[24] Z. Yao, L. Xiong, and H. Miao, "Ray-tracing based millimeter-wave channel characteristics in subway carriage," in *Proc. IEEE/CIC Int. Conf. Commun. China (ICCC)*, Aug. 2020, pp. 681–686, doi: 10.1109/ICCC49849.2020.9238950.

[25] W. Li, L. Liu, C. Tao, Y. Lu, J. Xiao, and P. Liu, "Channel measurements and angle estimation for massive MIMO systems in a stadium," in *Proc. 17th Int. Conf. Adv. Commun. Technol. (ICACT)*, Jul. 2015, pp. 105–108, doi: 10.1109/ICACT.2015.7224767.

[26] M. N. Islam, S. Subramanian, A. Partyka, and A. Sampath, "Coverage and capacity of 28 GHz band in indoor stadiums," in *Proc. IEEE Wireless Commun. Netw. Conf.*, Apr. 2016, pp. 1–7, doi: 10.1109/WCNC.2016.7564885.

[27] M. Schmieder, T. Eichler, S. Wittig, M. Peter, and W. Keusgen, "Measurement and characterization of an indoor industrial environment at 3.7 and 28 GHz," in *Proc. 14th Eur. Conf. Antennas Propag. (EuCAP)*, Mar. 2020, pp. 1–5, doi: 10.23919/EuCAP48036.2020.9135943.

[28] D. Dupleich, R. Müller, M. Landmann, J. Luo, G. D. Galdo, and R. S. Thomä, "Multi-band characterization of propagation in industry scenarios," in *Proc. 14th Eur. Conf. Antennas Propag. (EuCAP)*, Mar. 2020, pp. 1–5.

[29] S. Sun, G. R. MacCartney, and T. S. Rappaport, "Millimeter-wave distance-dependent large-scale propagation measurements and path loss models for outdoor and indoor 5G systems," in *Proc. 10th Eur. Conf. Antennas Propag. (EuCAP)*, Apr. 2016, pp. 1–5, doi: 10.1109/EuCAP.2016.7481506.

[30] IST-4-027756 WINNER II D1.1.2 V1.2. (Feb. 2008). *WINNER II Channel Models Part II*. [Online]. Available: http://www.ist-winner.org

[31] *Technical Specification Group Radio Access Network; Evolved Universal Terrestrial Radio Access (E-UTRA); Further Advancements for E-UTRA Physical Layer Aspects*, document TR 36.814 (Release 9), 3GPP, 2010.

**SATOSHI ITO** received the B.S. and M.S. degrees in electrical and electronic engineering from the Tokyo Institute of Technology, Tokyo, Japan, in 2013 and 2015, respectively. He joined KDDI Corporation, Tokyo, Japan, in 2015, and engaged in server maintenance and operation. Since 2016, he has been working with KDDI Research, Inc., Saitama, Japan. His main research interests include channel parameter estimation and propagation channel modeling in millimeter-wave frequency bands. He received the Young Researcher's Award from IEICE, in 2021.

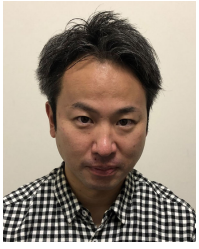

**TAKAHIRO HAYASHI** received the B.E. and M.E. degrees in information and communication engineering from Yokohama National University, Japan, in 2002 and 2004, respectively. In 2004, he joined KDDI Corporation, where he was engaged in telecommunication network planning and optimization. Since 2010, he has been engaged in the research and development of mobile communication systems with KDDI Research, Inc. He is currently involved in the development of new frequency bands and radio propagation prediction by using machine learning. He received the Young Researcher's Award from IEICE, in 2011.